

# NUMERICAL AND EXPERIMENTAL INVESTIGATION OF THE FLOWFIELD IN A BLOWDOWN WIND TUNNEL

Ali Rebaine, Mahmood Khalid, Cabot Broughton and Fred Ellis  
Institute for Aerospace Research, National Research Council  
Montreal Road, K1A 0R6, Ottawa, Ontario, Canada

**Keywords:** *Blowdown wind tunnel, High speed flow, Screens, Internal flow, Turbulent flow*

## Abstract

*This paper presents a numerical and experimental investigation of the flow field in a blowdown wind tunnel through the control-valve, the wide-angle diffuser, the settling chamber and the turbulence-damping screens. The computations are carried out using the Wind code on multi-block non-contiguous grids. The numerical results are compared to experimental measurements.*

## 1 Introduction

A blowdown intermittent wind tunnel typically provides test section conditions of constant Mach number and total pressure for a wind tunnel run of typically 5 to 30 secs duration [1]. The total pressure is maintained at a constant value by a servo controlled variable area valve. The valve area must change continuously during the blowdown to compensate for the change in pressure and density of the gas in the upstream storage vessel. The control valve may operate at pressure ratios of about 20 at the start of a run and approach unity at the end, thus leading to a wide variety of diffuser entry conditions. The maximum open area of the valve is typically chosen to be of the same order of magnitude as the test section cross-section area, while the "start of run" flow area can be of the order of 10% of the test section cross area. To efficiently provide good test section flow quality, the working fluid must be passed through devices such as screens, acoustical baffles, honeycomb, etc. (Figure 1) at low velocity prior to accelerating the flow towards

the test section conditions. To achieve this low velocity, the violent flow leaving the control valve must be diffused. It is appropriate to use a short wide-angle diffuser for that purpose. This type of diffuser is chosen in order to minimize the fill-up volume, diffuser material cost, real estate required and size of enclosing building. It also minimizes the time delay from the control valve to the settling chamber exit, which is important for pressure feedback control stability. In an effort to prevent unsteady flow separation in the rapidly expanding short diffuser, which could result in a poor velocity distribution, unsteady flow angularity and turbulence in the settling chamber, high-pressure loss flow spreaders are used. The actual design and geometries of valves and diffusers for a blowdown wind tunnel are diverse, each usually being unique to the facility or at least to the company designing the facility. Owing to the wide range of flow conditions experienced in the diffuser, the design of the flow-spreading devices in the diffuser are generally a compromise.

It is very difficult to observe or conduct extensive measurements of the flow in such a limited access environment (particularly at full scale). In an effort to improve the performance of the NRC 1.5m wind tunnel, CFD modeling and 1/12<sup>th</sup> scale experimental projects have been initiated to investigate the flow field in this component of the tunnel.

In a previous work [2], numerical simulation has been conducted to investigate the flow in the control valve and the wide-angle diffuser. The settling chamber was considered

as a tube, followed by a simple converging cone. The CFD demonstrated its capability to handle such a complicated flow. The present paper is an extension of this work. Two different configurations have been investigated. The first one consists of the current 1.5m tunnel configuration, which includes the conical centerbody. The second one does not include the conical center body. The numerical results have been compared to experimental measurements.

## 2 Grid generation

There were a number of challenges in being able to produce good grids. Owing to the complexity of the geometry and the demanding nature of the flow physics being simulated, a new procedure to generate a suitable grid was developed. From the previous work [2], we learnt more about the physics of the flow, which allowed us in the present work, to generate grids that could produce solutions more rapidly. Following the procedure developed in [2], a number of non-contiguous, multi-block grids have been generated for two different configurations. Figure 2 shows the grid for configuration 1, which is representative of the current 1.5m tunnel configuration. Figure 3 shows a generic grid without the conical body, which represents configuration 2. The grid density has been reduced for the purpose of visualization. Notice that axisymmetric flow has been assumed in the numerical model, and that the acoustical baffles have thus been eliminated in the simulation.

## 3 Numerical investigation

The flow field was considered axisymmetric and was numerically computed by solving the Reynolds averaged Navier-Stokes equations using the WIND code [3]. Roe's second-order flux-difference splitting scheme for the explicit (right-hand side) terms and a block matrix solver for the approximately factored implicit (left-hand side) terms were used. The Total-Variation-Diminishing (TVD) operator was used to prevent non-physical instabilities from

arising during the solution. Explicit boundary conditions were used.

The simulations were carried out for a total pressure of 185 psia and a total temperature of 528 °R at the inlet of the control valve. The downstream static pressure was computed to satisfy the desired mass flow rate. The unit Reynolds number, based on the inlet conditions, is about  $Re = 4.355 \times 10^6/\text{ft}$ . The screen boundary conditions were applied to simulate the discontinuities across the two porous plates and the seven turbulence-damping screens. The geometric open area ratio of the upstream plate is 44% and that of the downstream plate is 23%, whereas the open area ratio for the first six screens is 46.2%, and for the last one is 57.8%. The total pressure losses across each plate and screen are determined throughout the computation using Cornell's correlation [4]. The viscous and adiabatic conditions were imposed on all the solid walls and a slip boundary condition was applied on the symmetry axis. The average Navier-Stokes equations were solved using the SST turbulence model [5]. The computations were started from the uniform flow field corresponding to a very low total pressure. Sequential runs without representing the porous plates and the turbulence damping screens were then carried out by slowly increasing the inlet total pressure up to the specified value. Then the screen boundary conditions were implemented in stages, starting from a low value of solidity equal to 0.1 to the geometric values. This procedure was adopted to bypass any sudden shock problem. The computations were then continued until convergence to the steady state was reached. This corresponds to a balanced mass flow rate between the inlet and the outlet of the domain. It was found that if the geometric porosity value was used for the second perforated plate, physically impossible flows were predicted and the flow solver could not converge the solution. The second perforated plate porosity factor of 40% was then determined as an appropriate value, as this gave reasonably close agreement between the numerical and experimental pressure losses over the complete wide-angle diffuser.

#### 4 Experimental investigation

The experimental investigations were carried out in both the 1.5m tunnel and in a 1/12<sup>th</sup> scaled blowdown wind tunnel model. The Oil dot surface flow viz technique was used in the full-scale facility to visualize the flow field within the inlet of the wide-angle diffuser (Figure 7). Note: The oil flow visualization in the 1.5m tunnel was not for the exact conditions of the numerical study. The oil dots were placed on the surface in advance of the run, and the run was carried out over a range of air storage tank pressures. During the run the control valve would have assumed a range of openings as the upstream pressure dropped. The measurements of the Mach number profiles were done along three traverse stations (see Figure 1) in the wide-angle diffuser of a 1/12<sup>th</sup> scale pilot tunnel. These measurements were obtained by traversing a “forward” facing and “aft” facing Pitot probe assembly. The experimental data was found to be repeatable, but is subject to several significant error sources. The local direction of the flow was unknown, thus the flow direction was assumed to be roughly aligned with the axis of the Pitots of the probe assembly. Downstream flow was assumed when the forward facing Pitot registered a higher pressure than the aft facing Pitot and vice versa. The local static pressure was determined by using the downstream (as determined by the above method) base pressure Pitot measurement and a calibration factor determined over a range of Mach numbers in a known uniform flow. The calibration factors were determined for a range of flow angles (relative to the Pitot assembly axis), and the factors were found to be relatively constant for flow angles of up to +/-30 degrees.

#### 5 Results and discussion

The computations show that the flow through the valve throat is choked and that the emerging jet contains complex interacting oblique shock and expansion wave patterns (Figures 4 and 5). This was expected given the pressure ratio of the jet. The mean value of the pressure ratio (static/total) at this section is about 0.46.

In configuration 1, the violent high-energy jet is deflected by the conical centerbody (Figure 6). The shearing action of the redirected free jet produces three strong toroidal shaped recirculating zones, upstream of the first perforated plate. The first toroid fills the area bounded by the valve sleeve, valve housing internal surfaces, and the jet from the valve to the conical centerbody. The wide-angle diffuser wall, the jet from the valve, and the redirected jet to the first perforated plate bound the second toroid. The third recirculating toroid is found in the base area of the conical center-body. Oil dots surface flow visualizations from the 1.5m wind tunnel shown in Figures 7 generally support the CFD predicted flow field, upstream of the first perforated plate where the first toroid is presented in Figures 7a and 7c, the second one in Figure 7a and the third one in Figure 7b. Between the first and the second perforated plates, the flow is found to be still like a free jet. Downstream of the second perforated plate, the numerical results show a more diffused flow. The total pressure predicted by the CFD in the settling chamber is about 20 psia.

In configuration 2, the annular violent high-energy jet converges to the centerline where it is deflected upstream of the first perforated plate (Figure 8). This induces the generation of two recirculating toroids. The one which fills the area bounded by the valve sleeve, valve housing internal surfaces, and the jet from the valve to the centerline. The other one is bounded by the wide-angle diffuser wall, the jet from the valve, and the redirected jet to the first perforated plate. Between the first and the second perforated plates, the jet continues spreading close to the centerline. Again, as for configuration 1, the numerical results predict a more diffused flow downstream of the second perforated plate. The total pressure predicted in the settling chamber is about 19 psia.

Figures 9 and 10 show a comparison between the computed and measured Mach number distributions at stations A, B and C (see Figure 1) for configuration 1 and 2, respectively. The overall trends in terms of distributions, magnitudes and peak locations are well captured for configurations 1 at upstream

stations A and B. For downstream station C, which is immediately downstream of the recirculating zones, the comparison is qualitatively satisfactory. For configuration 2, which does not contain a conical centerbody, there is a noticeable offset between the computed and measured profiles at station B. Since the flow in configuration 2 is not as much diffused as in configuration 1, the comparison between Mach number profiles at station C is encouraging.

The plots of Figure 11 are velocity vector predictions on radial cuts at three axial stations in the cylindrical section of the settling chamber. The first is at the inlet of the settling chamber, the second is just upstream of the 1<sup>st</sup> turbulence reduction screen, and the third is just downstream of the 7<sup>th</sup> turbulence reduction screen. Configuration 1 (with the conical centerbody) is shown in blue, while the red vectors are for configuration 2 (without the conical centerbody). At the inlet to the settling chamber, it is fairly clear that the conical centerbody produces a double-hump, wake-type profile (annular jet), while configuration 2 has a core flow profile. Although the centerbody produces the more uniform inlet velocity profile, there appears to be a fairly strong trend to accentuate the perimeter velocities, which result in significant inward redistribution of the flow at the entrance to the first screen. Although the core flow of configuration 2 appears to be progressing towards a more uniform profile, there is insufficient length for this to be completed, and at the first screen, significant redistribution of the flow towards the perimeter results. Within this range of inlet velocity profiles, the seven turbulence reduction screens are predicted to produce essentially uniform exit velocity profiles.

## 6 Conclusions

The CFD option provides a reliable means of studying complex flows in not so easy to access sections of the tunnel.

The numerically predicted flow field from the control valve up to the second perforated

plate is in good agreement with the experimental measurements and observations.

Downstream from the second perforated plate, the CFD predicts a more diffused flow than the measured one.

## References

- [1] Pope A., and Goin K. L., *High-Speed Wind Tunnel Testing*, John Wiley and Sons, Inc., 1965.
- [2] Rebaine A., Khalid M., Broughton C. and Ellis F., Numerical Flow Simulation of a Blowdown Wind Tunnel Control Valve Wide Angle Diffuser with Comparison to Scaled Experimental Model, *CASI, 48<sup>th</sup> Annual Conference*, April 29 - May 2, 2001.
- [3] *WIND code manuals*, the NPARC Alliance, NASA Glenn Research Center, Cleveland, Ohio, <http://www.lerc.nasa.gov/www/wind>.
- [4] Cornell, W. G., Losses in Flow Normal to Plane Screens, *Transaction of the ASME*, vol. 80, pp. 791-799, 1958.
- [5] Menter Florian R., Zonal Two Equation  $k-\omega$  Turbulence Models for Aerodynamic Flows, *AIAA paper*, 93-2906, July 1993

NUMERICAL AND EXPERIMENTAL INVESTIGATION  
OF THE FLOWFIELD IN A BLOWDOWN WIND TUNNEL

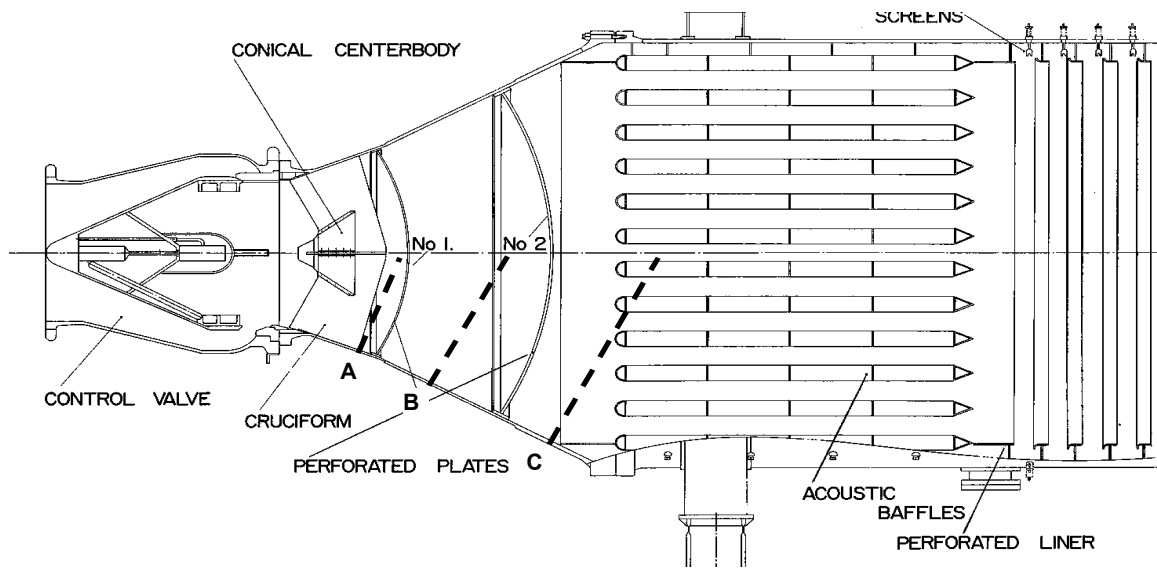


Figure 1. Cross-Section of the 1.5m NRC/IAR Wind Tunnel Pressure Control Valve, Wide Angle Diffuser, and a portion of the Settling Chamber. Heavy dashed lines are approximate locations of the experimental Pitot Traverses and the CFD simulation comparison data cut

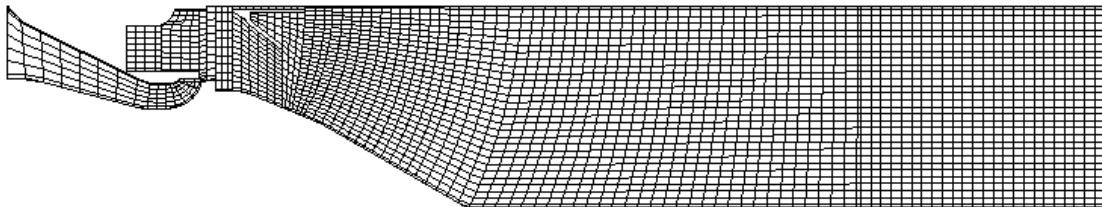


Figure 2. Non-contiguous structured multi-block grid for the configuration 1.

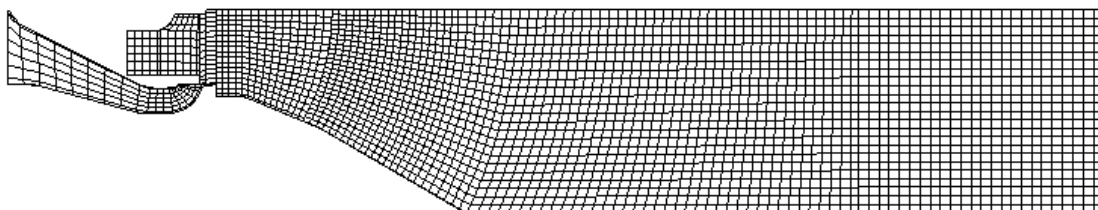


Figure 3. Non-contiguous structured multi-block grid for the configuration 2.

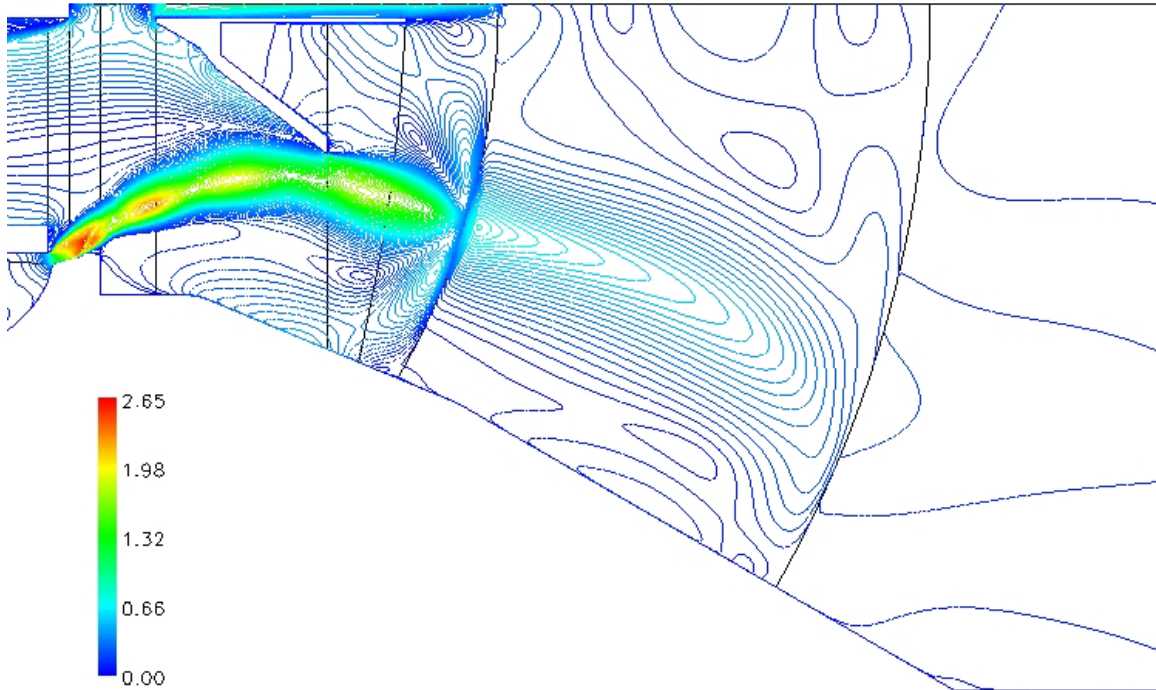


Figure 4. Mach number contours in the configuration 1.

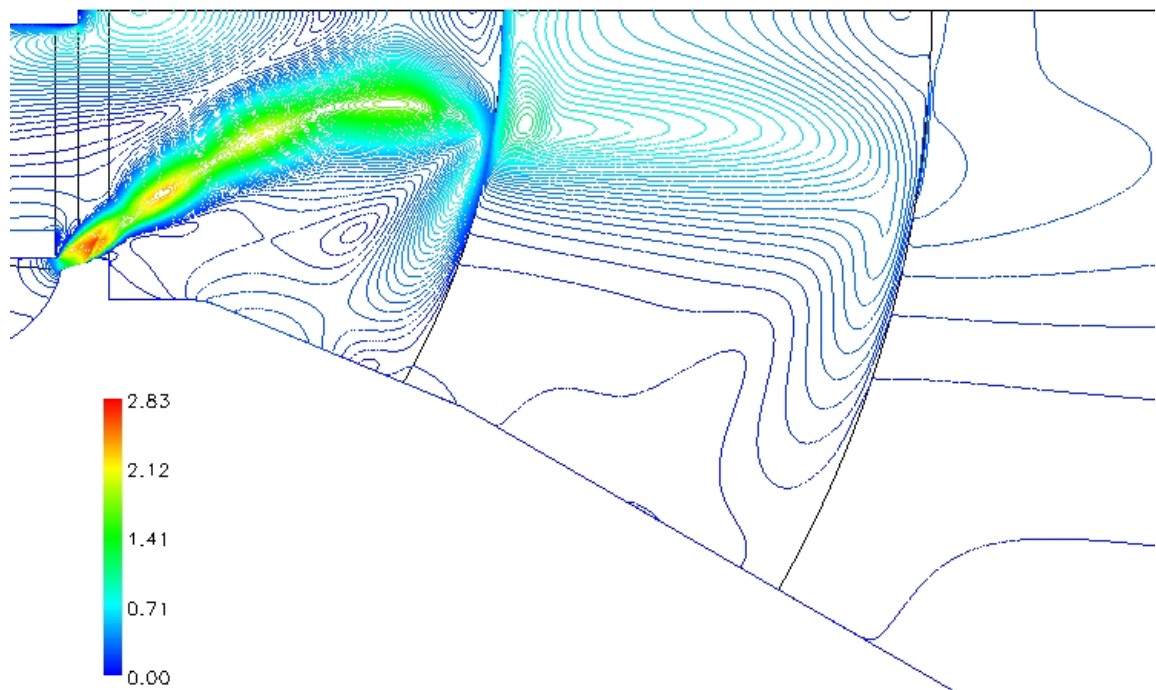


Figure 5. Mach number contours in the configuration 2

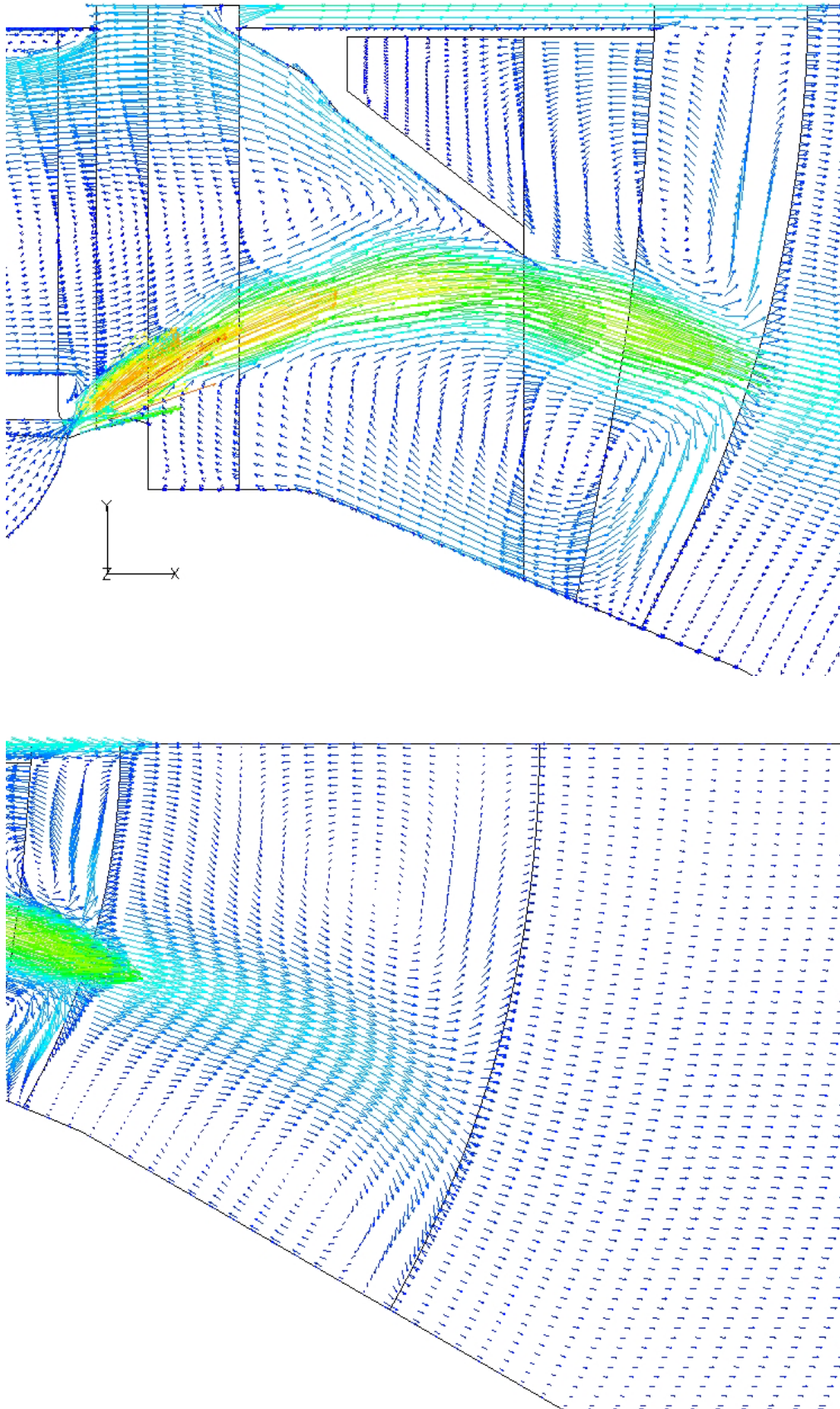
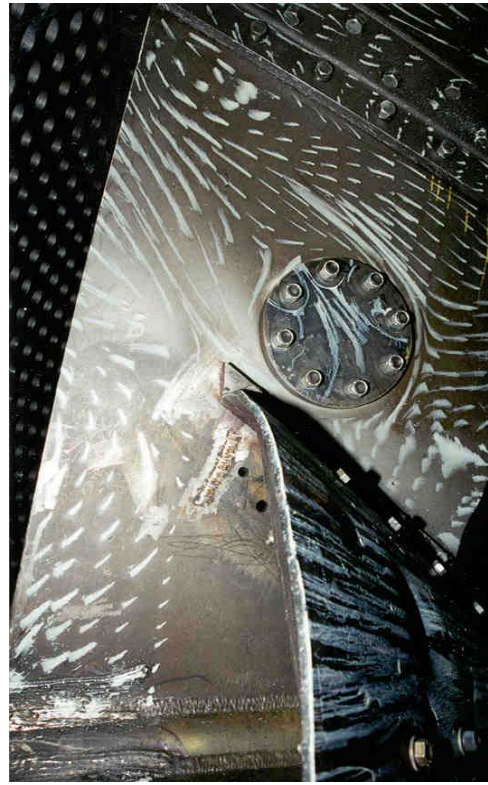


Figure 6. Flow field in the configuration 1.



a



b



c

Figure 7. Oil dots surface visualization in the configuration 1.

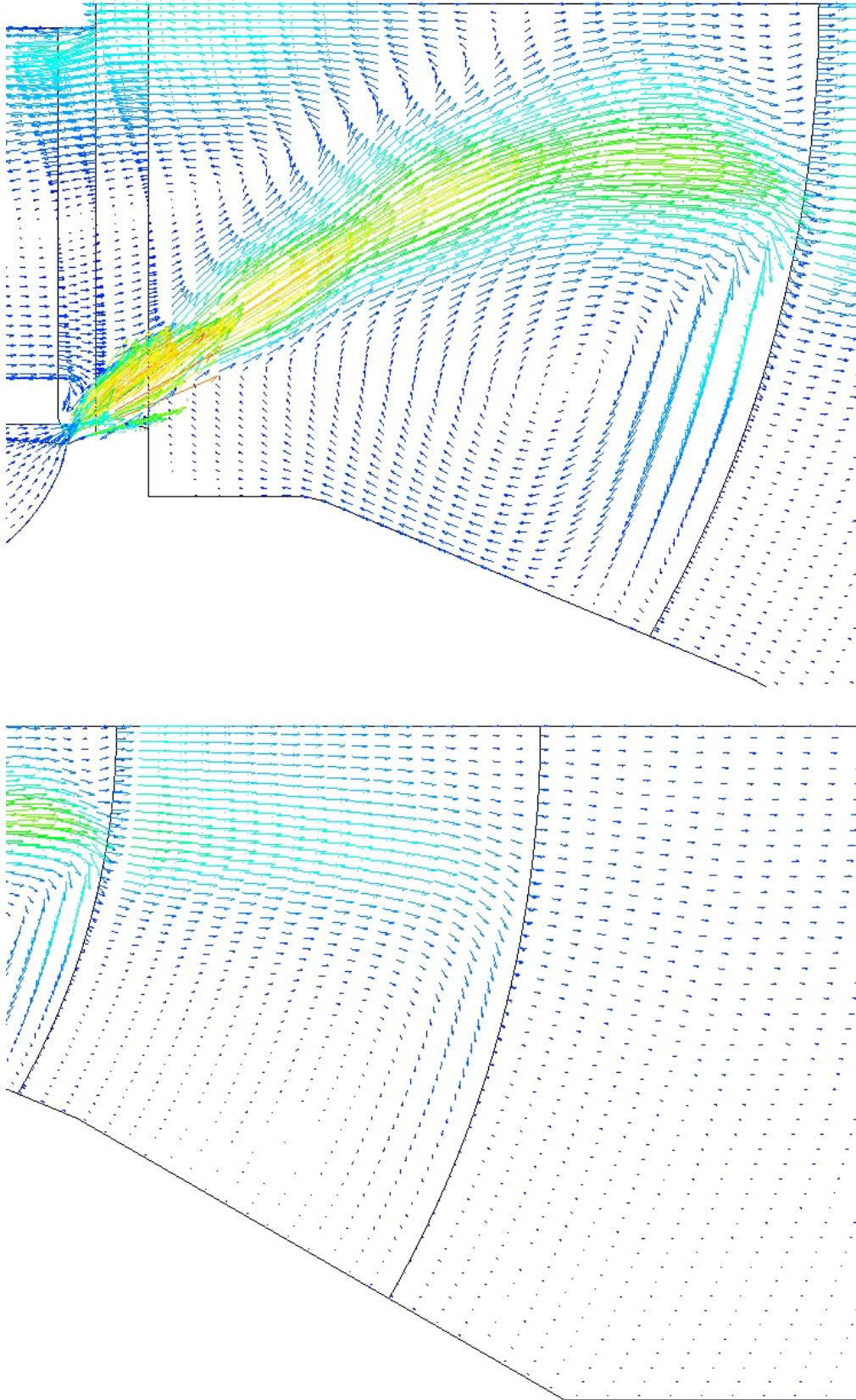


Figure 8. Flow field in the configuration 2.

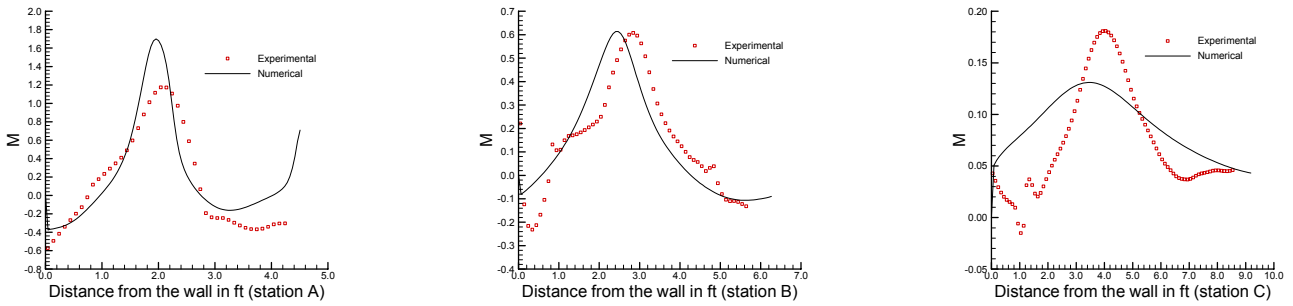


Figure 9. Mach number at three cross-stations in the wide-angle diffuser of the configuration 1.

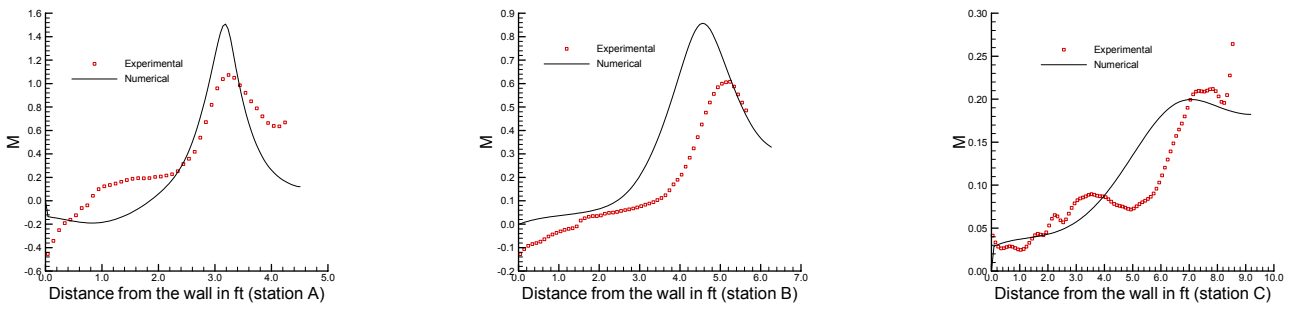


Figure 10. Mach number at three cross-stations in the wide-angle diffuser of the configuration 2.

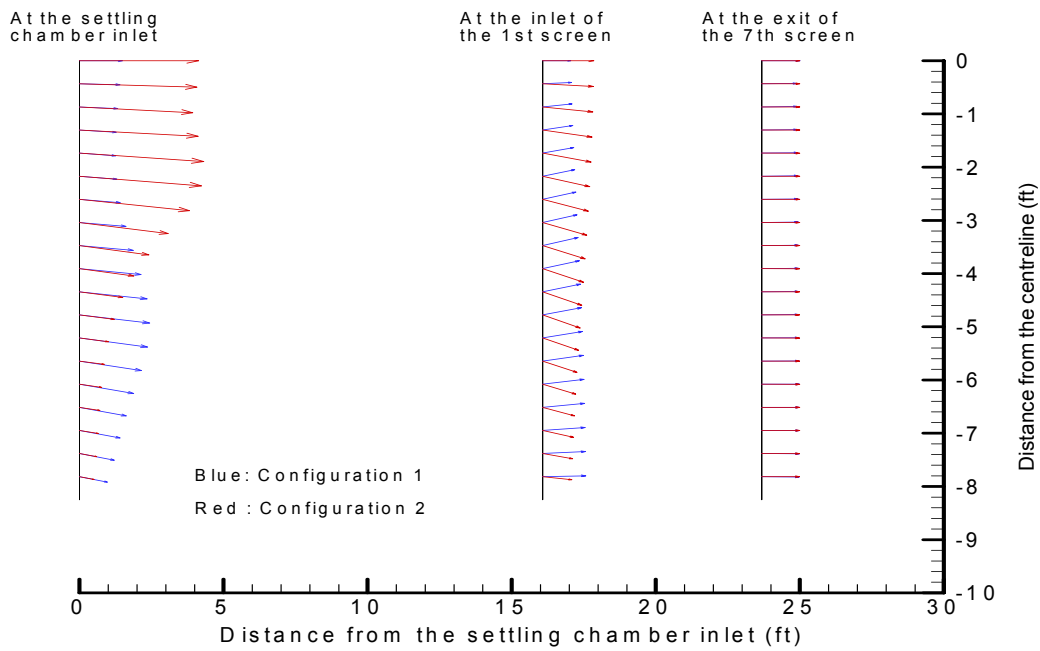


Figure 11. Flow angularities comparison in the configuration 1 and 2